Flapping motion in 2D: experimental and numerical analysis

E. Sarıgöl* and N. Alemdaroğlu*

*Middle East Technical University

Aerospace Engineering Department 06531 Ankara, Türkiye

Abstract

Flapping motion has several advantages in low Reynolds number regime. These advantages are their ability to reach very high unsteady lift coefficients and to hover. Unsteady analysis of a flapping airfoil in hover at low Reynolds number regime in an incompressible flow is performed to investigate the physics of flapping motion. Experimental analysis is carried out using Particle Image Velocimetry (PIV) technique and numerical analysis is done using a commercially available Direct Numerical Simulation (DNS) tool (STAR-CD) to solve the laminar flow Navier-Stokes equations on a moving grid. The velocity fields obtained from PIV experiments are compared with the one obtained numerically. The experimental work is used to validate the numerical results and show their reliability.

1. Introduction

In recent years, flapping motion has attracted a lot of attention because of its advantages in low Reynolds number regime. These advantages are its ability to reach very high unsteady lift coefficients and therefore to be able to hover. Aerodynamics of hovering insect flight has been investigated by many researchers. Ellington in a series of papers evaluated the quasi-steady and unsteady aerodynamic mechanisms¹⁻³. In recent years, experimental research on the flapping motion is performed mostly by using the so called "Digital Particle Image Velocimetry (DPIV)" technique. Lehmann et al. used DPIV to investigate force enhancement due to contralateral wing interactions during stroke reversal (the clap-and-fling) on a dynamically scaled mechanical model of a small fruit fly, *Drosophila Melanogaster*⁴. Dickson and Dickinson used a dynamically scaled model of the same species to measure the forces produced by a wing revolving at constant angular velocity while simultaneously translating at velocities appropriate for forward flight⁵. Warrick et al used DPIV to visualize the flow field around the wake of a hovering hummingbird, *Selasphorus Rufus*. In their study, they presented the evidence of leading edge vortices created during the downstroke⁶. The rotational forces produced by a flapping insect wing were investigated on a dynamically scaled model insect by Sane and Dickinson. The aim was to characterize the effect of wing rotation on an aerodynamic force generation for insect flight⁷.

On the other hand, numerical studies covered mainly the simulations of robotic wings or dynamically scaled models of insects. Aonou and Liu performed a multi-block and overset grid-based computational fluid dynamics (CFD) study for the unsteady flows about a realistic body-wing model and the force-generation in the flapping flight of the hawkmoth hovering based on real flight data⁸. Wang solved the Navier-Stokes equations in elliptic coordinates for an elliptic wing in order to quantify the vortex dynamics that is essential for hovering and identify a minimal two dimensional model that produces sufficient lift. The vortex dynamics further elucidates the role of the phase relation between the wing translation and rotation in lift generation and explains why the instantaneous forces can reach a periodic state after only a few strokes⁸⁻⁹. Miller and Peskin¹⁰ used the immersed boundary method to solve the twodimensional Navier-Stokes equations for two immersed wings performing an idealized 'clap and fling' stroke and a 'fling' half-stroke for Reynolds numbers between 8 and 128. Lewin and Haj-Hari presented a numerical model for two-dimensional flow around an airfoil undergoing prescribed heaving motions in a viscous flow to find the flow characteristics and power coefficients for both periodic and aperiodic solutions. They also discussed the importance of viscous effects for low-Reynolds-number flapping flight¹¹. Numerical simulations of hovering flapping motion for simplified wing configurations have been investigated by Sarigöl et al. for different kinematic patterns; i.e. effect of profile thickness and camber. The thickness of profile had an unfavorable effect on lift and drag coefficients for symmetrical profiles whereas the presence of camber increased the aerodynamic force coefficients compared to symmetrical profiles ¹³⁻¹⁴.

This study presents an unsteady analysis at low Reynolds number regime for a flapping airfoil on a rectangular cambered wing, NACA 6412, in incompressible flow. The aim is to investigate the physics of flapping motion in hover. The flapping motion is analyzed experimentally using the Particle Image Velocimetry (PIV) technique and numerically using a commercially available Direct Numerical Simulation (DNS) tool (STAR-CD) by solving the

Navier-Stokes equations for laminar flow on a moving grid. The velocity field obtained from PIV measurements is compared with the one obtained from numerical studies. In a way, experimental work is used to validate the results and show the reliability of the numerical simulations.

2. Methods

The flapping motion consists of two translational phases (upstroke and downstroke) and two rotational phases (pronation and supination). In translational phases, wings sweep through air with a high angle of attack whereas in the rotational phases wings rapidly rotate and reverse direction. One period of motion is defined in terms of four regions each of which including one translational and one rotational phases. During the rotation of the profile, the leading edge stays as the leading edge. Hovering is an extreme mode of flight where the forward velocity is zero.

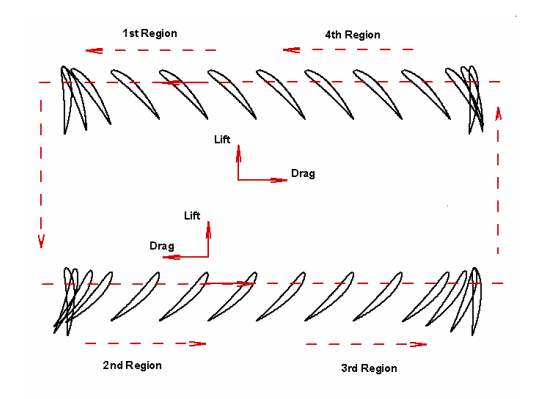


Figure 1: Definition of flapping motion.

2.1 Numerical Method

The pressure and the velocity fields are obtained via the solution of two-dimensional time-dependent Navier-Stokes equations in laminar, incompressible flow. The mass and momentum conservation equations for general incompressible and compressible fluid flows and a moving coordinate frame are given by:

$$\frac{1}{\sqrt{g}} \frac{\partial}{\partial t} \left(\sqrt{g} \, \rho \right) + \frac{\partial}{\partial x_j} \left(\rho u_j \right) = 0 \tag{1}$$

$$\frac{1}{\sqrt{g}} \frac{\partial}{\partial t} \left(\sqrt{g} \rho u_i \right) + \frac{\partial}{\partial x_j} \left(\rho u_j u_i - \tau_{ij} \right) = -\frac{\partial p}{\partial x_i}$$
 (2)

where the constitutive relation is given by

$$\tau_{ij} = 2 \mu s_{ij} - \frac{2}{3} \left\{ \mu \left(\frac{\partial u_k}{\partial x_k} \right) \delta_{ij} \right\} \text{ with } s_{ij} = \frac{1}{2} \left(\frac{\partial u_i}{\partial x_j} + \frac{\partial u_j}{\partial x_i} \right).$$

O-type grids are used around the airfoil (Figure 2) to simulate the motion. The computational domain is moved and rotated by user-defined subroutines. The grid domain consists of approximately 30000 cells and the outer boundary is located at 15c. The computational domain consists of a single domain in which the grid is generated by hyperbolic method. The velocity of the motion is defined with respect to the center of rotation and no-slip boundary condition is applied on the airfoil surface. Since STAR-CD is a finite volume solver, the front and back side of the computational domain is defined with the symmetry boundary condition. The farfield is implied by setting pressure boundary condition for incompressible flow with constant density and viscosity.

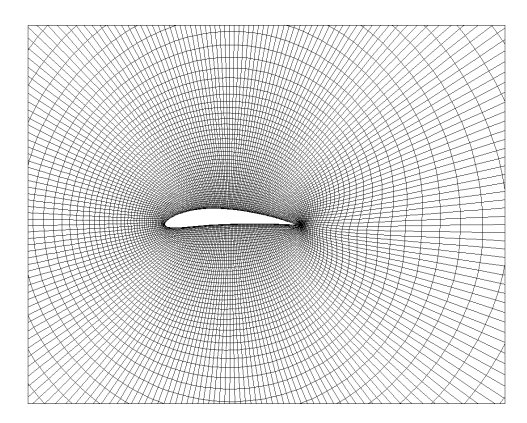


Figure 2: Computational mesh around NACA 6412.

At Re=1000, the flow is assumed to be laminar and incompressible (Mach=O(10⁻³)). Therefore no turbulence model is used and therefore the simulation is time-accurate or Direct Numerical Simulation (DNS). The pressure-velocity coupling in incompressible flow simulations is obtained using the iterative Pressure Implicit with Splitting Operators (PISO) scheme.

2.2 Experimental Method

Experimental visualization of velocity field around the cambered airfoil NACA 6412 is done using the PIV technique. The experiments are carried out in a 1.5m x 1m x 1m water tank which is seeded with hollow glass spheres for laser illumination. The model is transparent and the defined motion is implemented using a PLC server. The schematic representation of the experimental setup is given in Figure 3. Two-dimensional visualization of the hovering flapping motion is done at the mid-span of the profile. The plane at mid-span is illuminated by a double-pulsed Nd:YaG laser and the two CCD cameras operating in a synchronized manner take two successive pictures at each pulse of the laser. The velocity fields are then calculated using adaptive correlation between the two images taken.

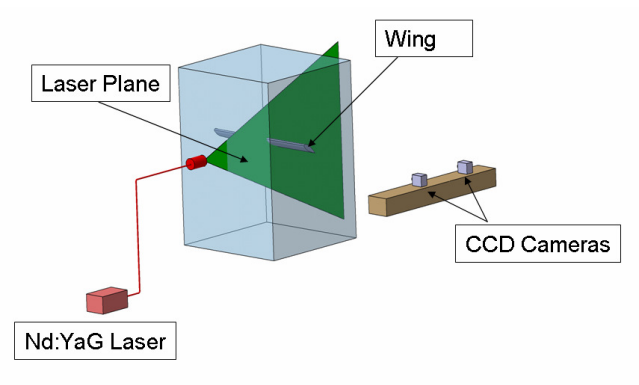


Figure 3: Schematic representation of experimental setup.

2.3 Vortex Identification

Although vortices are observed in almost every branch of fluid dynamics, no precise definition of it has been proposed yet. According to Jeong and Hussain¹⁵ a vortex should at least possess the following properties: (i) a vortex core must have a net vorticity, consequently a net circulation. (ii) The geometrical characteristics of a vortex core must be Galilean invariant.

There has been a number of methods proposed to identify the vortices. Many researchers used the magnitude of vorticity, $|\omega|$, as an indicator. However, the use of $|\omega|$ may be misleading because this technique can not distinguish between the rotation due to pure shear and rotation due to an actual swirling motion. Pressure is another scalar indicator for vortex identification. For a steady, inviscid, planar two-dimensional flow, pressure shows a minimum at the center of circular pattern but this method is also shown to fail when the flow is unsteady or three-dimensional ¹⁵.

For an incompressible flow, the second invariant of velocity gradient tensor can be written in terms of symmetric (deformation tensor, S) and anti-symmetric (rotation tensor, Ω) parts.

$$S = \frac{u_{i/j} + u_{j/i}}{2} \text{ and } \Omega = \frac{u_{i/j} - u_{j/i}}{2}$$
 (3)

The Q criterion, proposed by Hunt et al¹⁷ identifies the vortex regions with positive second invariant of velocity gradient., ∇u ; i.e. Q > 0

$$Q = \frac{1}{2} \left\| \Omega \right\|^2 - \left\| S \right\|^2 \right) \tag{4}$$

where $\|\Omega\| = [tr(\Omega\Omega^T)]$ and $\|S\| = [tr(SS^T)]$. Additionally, the pressure in the eddy region is required to be lower than the ambient pressure. This additional condition makes the criterion independent of the sign of Q and it is related to pressure by:

$$\nabla^2 p = 2\rho Q \tag{5}$$

There is no explicit connection between a region with $Q \ge 0$ and a region containing a pressure minimum. In an incompressible flow, Q is a local measure of the excess rotation rate relative to the strain rate¹⁹. It should be noted that Q > 0 does not guarantee the existence of a pressure minimum inside the region identified by it¹⁵. The use of Q criterion without the additional pressure condition is also done in the literature and is acceptable¹⁹. The relation (4) shows that the quantity Q represents a local balance between the rotation and deformation rates of a fluid element. This is the same definition of a vortex that has been formulated by Chong¹⁶ a vortex is a connected region where the antisymmetric component of ∇u predominates over the symmetric one.

Another method to identify the vortex regions is λ_2 criterion proposed by Jeong and Hussain¹⁵. Since $S^2 + \Omega^2$ is symmetric then the eigenvalues of this tensor are real. For two-dimensional flow, if the eigenvalues of the symmetric tensor $S^2 + \Omega^2$ are ordered as $\lambda_1 \geq \lambda_2$, then the second largest eigenvalue should be negative which is equivalent to saying that $\lambda_2 < 0$ at every point inside the vortex core. Thus, this method is referred as the λ_2 criterion. The λ_2 criterion removes the main causes of inaccuracy, i.e. unsteady effects and viscous effects. Jeong and Hussain defined the vortex core as a connected region with two positive eigenvalues of the pressure Hessian to capture the region of local pressure minimum in a plane. Moreover these eigenvalues are related to Q by

$$Q = -\frac{1}{2} \left(S^2 + \Omega^2 \right) = -\frac{1}{2} \left(\lambda_1 + \lambda_2 \right)$$
 (6)

From Jeong and Hussain, it can be shown that while Q criterion measures the excess rate of rotation over the strain magnitude in all directions, the λ_2 criterion looks for this excess only on a specific plane¹⁵. The point of local pressure minimum in a plane requires two eigenvalues of the local pressure Hessian to be positive and the local pressure gradient component on the plane to be zero. The region in which the two eigenvalues of the pressure Hessian are positive is thus less restrictive and may not include the point of planar pressure minimum in its interior (if there does not exist a point of vanishing pressure gradient on the plane). Furthermore, the relationship between the actual and the modified pressure distribution that neglects the unsteady and viscous terms is not clear ¹⁹. Also, the pressure Hessian concept defined above is not applicable for the case of compressible flows because of non-vanishing density gradient and divergence of velocity¹⁸. Hussain et al. used Q and λ_2 criteria to deduce coherent vortices from the flow field. Higher positive values of Q signifying dominance of rotation over strain are representative of coherent structures⁶. As stated by Dubief et al.¹⁹ the choice of the Q criterion as a vortex identification method is strongly supported by: its relation to pressure low, the very definition of Q, as the balance between the local rotation rate and strain rate. The λ_2 approach proposed by Jeong and Hussain¹⁵ has proven to be an effective technique for locating vortex cores in many real-world applications. However, the problems such as the

appearance of discontinuous line segments and the influence of a curling flow require that the underlying theory be revisited²².

3. Results

The paper presents the experimental results for a cambered airfoil, NACA 6412, at various angles of attack and compares the experimental results with the numerical simulations. The cyclic lift obtained during the flapping motion in hover is calculated and is further related to the vortices formed during different phases of flapping motion. As mentioned in literature, higher lift coefficients are obtained as the angle of attack is increased.

The qualitative comparison of flow topology between numerical and experimental results is done in terms of vortex identification methods described above (i.e. $|\omega|$, Q-criteria and second eigenvalue of velocity gradient). The leading and trailing edge vortices are identified and tracked at different phases of the motion and their effect on lift and drag coefficients are investigated. The simulations are carried out for different starting angles of attack. There are two lift generating mechanisms during the upstroke. These are the delayed stall and rotational lift generation mechanisms. Delayed stall is a translational mechanism where a vortex formation is observed at the leading edge during the first quarter period of the flapping motion. On the other hand, rotational lift generation is observed only during the pronation part of the flapping motion. During the downstroke phase, which is the second and third quarter periods of simulations, lift is generated due to the so called "wake capture" mechanism.

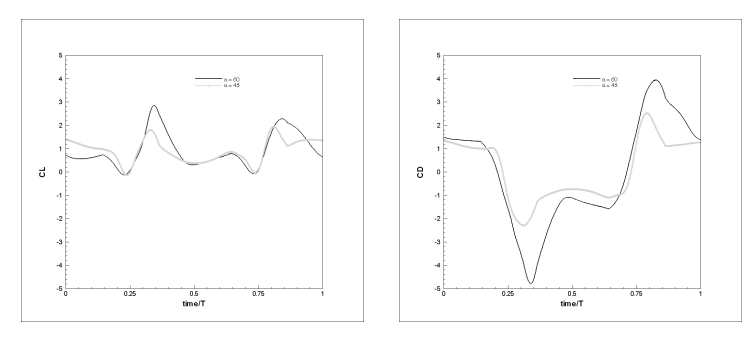


Figure 4: Lift (left) and drag (right) coefficients variation in one period for different angles of attack.

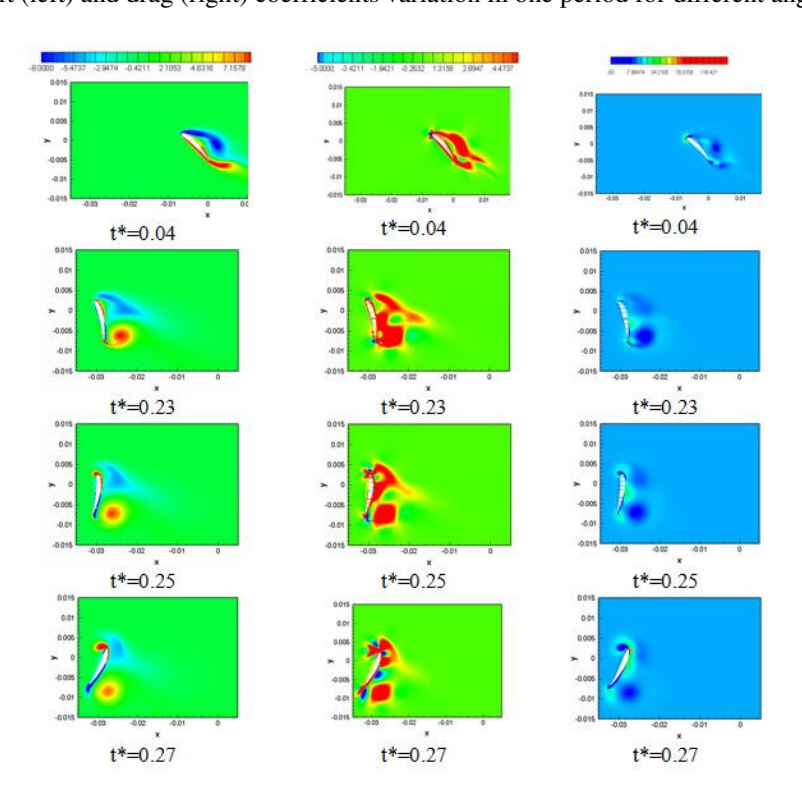


Figure 5: Numerical non-dimensional vorticity contours (1st column), Q contours (2nd column) and λ_2 contours (3rd column) at α =45° for the first quarter period.

In figures (5-8), the qualitative comparison of experimental data with numerical results is shown. The comparison is given for the first quarter period at specified non-dimensional time steps ($t^*=t/T_{per}$). The formation and the evolution of leading and trailing edge vortices are clearly identified both by Q (warm colors) and λ_2 techniques (cold colors). Although $|\omega|$ is not a dependable method compared to other two techniques to identify the vortex regions, it works reasonably well in this study. In the numerical simulations the fluid is air whereas in the experiments it is water. The flow is assumed to be laminar but it seems there is free stream turbulence in the experiments which is inevitable. This may be the reason for the quicker diffusion of vortices compared to numerical results. Numerical results are taken after the 6th period in order to avoid any left over effects of the impulsive start. This dry run period is significantly larger for the experiments. During the experiments, the results are taken after 15-20 periods have elapsed in order to obtain the periodicity of the flow. The particles, which should normally be suspended in water when there is no motion, show motion in stagnant regions. The translational velocity of the profile is calculated at Reynolds number 1000 assuming that the density and the viscosity of water are constants. However, it should be kept in mind that the viscosity of water depends on the temperature of the environment, which may be changing. This may be another reason for the rapid diffusion of vortices in water when compared to numerical simulations.

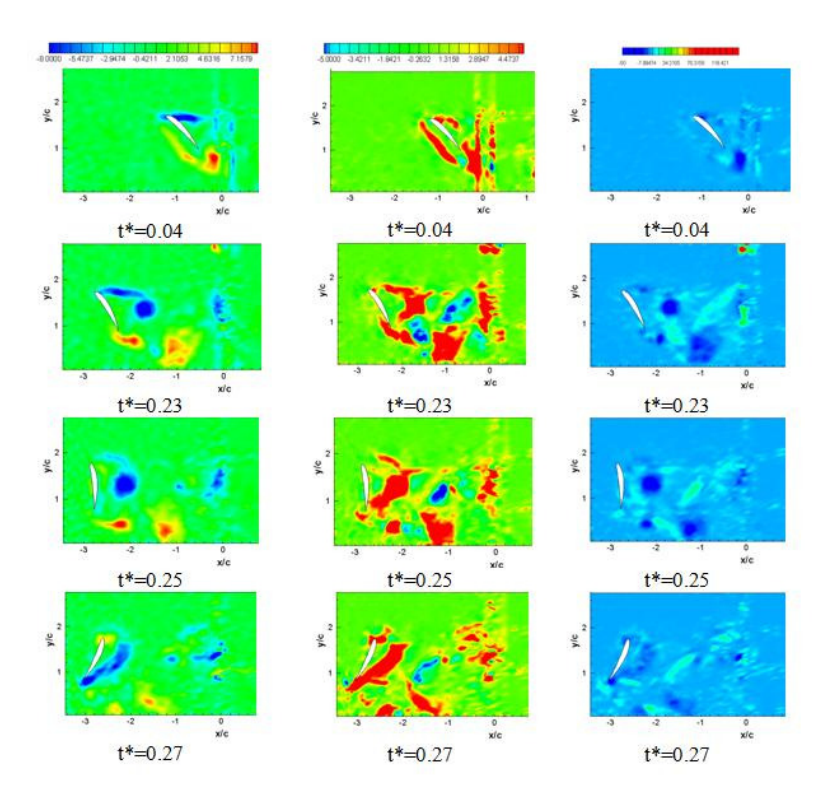


Figure 6: Experimental non-dimensional vorticity contours (1st column), Q contours (2nd column) and λ_2 contours (3rd column) at α =45° for the first quarter period.

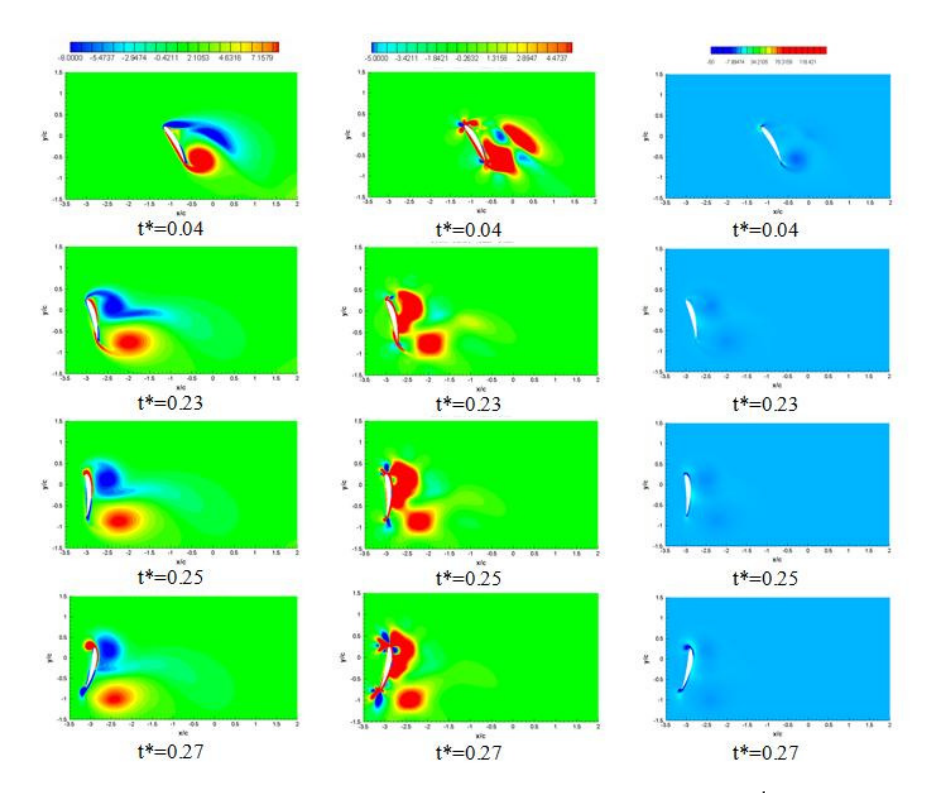


Figure 7: Numerical non-dimensional vorticity contours (1st column), Q contours (2nd column) and λ_2 contours (3rd column) at α =60° for the first quarter period.

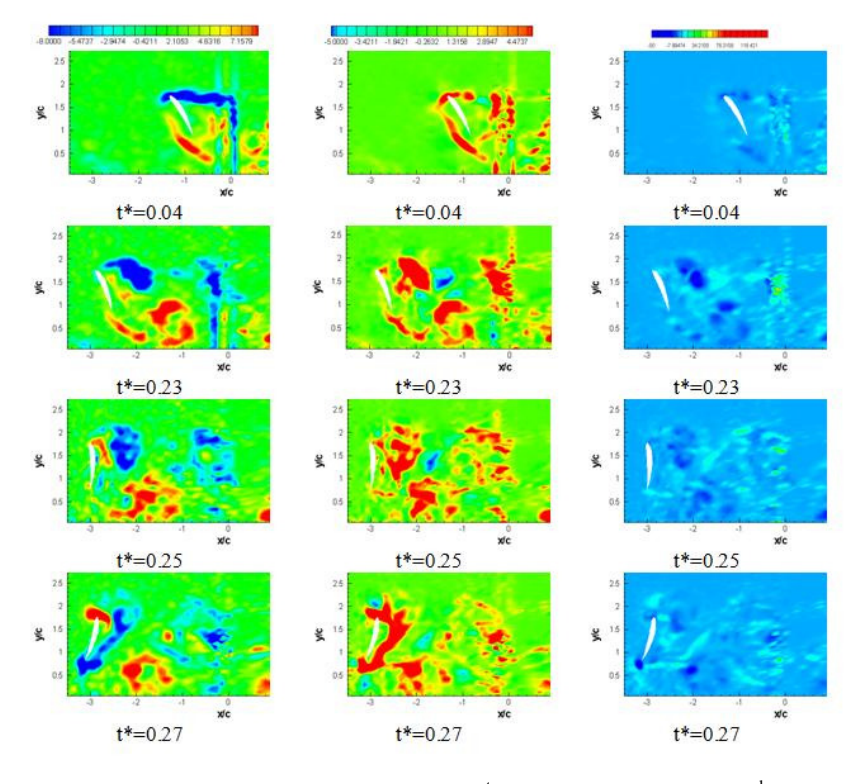


Figure 8: Experimental non-dimensional vorticity contours (1st column), Q contours (2nd column) and λ_2 contours (3rd column) at α =60° for the first quarter period.

4. Conclusions

Numerical and experimental investigations of hovering flapping motion at Re=1000 have been presented for two different starting angles of attack. Formation and evolution of leading and trailing edge vortices are clearly observed from both experimental and numerical simulations. The experiments prove that the numerical simulations can be dependable for future studies. Three dimensional simulations of hovering flapping motion are being currently investigated.

Acknowledgements

This research was supported by Technological and Research Council of Turkey, TUBİTAK under project number 104M417. The author E. Sarıgöl would like to thank to Asst. Prof. Dr. Serkan Özgen and Yüksel Ortakaya for their valuable comments.

References

- [1] Ellington, C.P. The Aerodynamics of Hovering Insect Flight I. The Quasi-Steady Analysis *Phil. Trans. R.Soc. Lond. B*, 305: 1-15, 1984.
- [2] Ellington, C.P. The Aerodynamics of Hovering Insect Flight IV Aerodynamic Mechanisms *Phil. Trans. R.Soc. Lond. B*, 305, No. 1122: 79-113, 1984.
- [3] Ellington, C.P. The Aerodynamics of Hovering Insect Flight V A Vortex Theory *Phil. Trans. R.Soc. Lond. B*, 305, No. 1122: 115-144, 1984.
- [4] Lehmann, F.O., Sane, S.P. and Dickinson, M. The aerodynamic effects of wing-wing interaction in flapping insect wings, *J. Exp. Biol.*, 208: 3075-3092, 2005.
- [5] Dickson, W.B. and Dickinson, M.H. The effect of advance ratio on the aerodynamics of revolving wings *J. Exp. Biol.*, 207, 4269-4281, 2004.
- [6] Warrick, D.R., Tobalske, B.W. and Powers, D.R. Aerodynamics of the Hovering hummingbird, *Nature*, 435,23, 1094-1097, 2005.
- [7] Sane, S.P. and Dickinson, M.H. The Aerodynamic effects of Wing Rotation and a Revised Quasi-Steady Model of Flapping Flight, *J. Exp. Biol.*, 205: 1087-1096, 2002
- [8] Aono, H. and Liu, H. Vortical Structures and Aerodynamics of Hawkmoth Hovering, *Journal of Biomechanical Science and Engineering*, 1, No.1: .234-245, 2006
- [9] Wang, Z. J. Dissecting Insect Flight Annu. Rev. Fluid Mech., 137: 183-210, 2005.
- [10] Wang, Z. J. Two Dimensional Mechanism for Insect Hovering *Physical Review Letters*, 85, No. 10, September 2000.
- [11] Miller, L.A. and Peskin, C.S. A Computational Fluid Dynamics of 'clap and fling' in the Smallest Insects *J. Exp. Biol.*, 208: 195-212, 2005.
- [12] Lewin, G.C. and Haj-Hari, H. Modelling Thrust Generation of a Two-Dimensional Heaving Airfoil in a Viscous Flow *J. Fluid Mech.*, 492: 339-362, 2003.
- [13] Sarıgöl, E. Kurtulus, D.F. and Alemdaroğlu, N. Çırpan Kanat Probleminde Kanat Profili Kalınlığının Sayısal İncelenmesi (in Turkish)", Proc. of HaSeM'06 International VI. Kayseri Aeronautical Symposium, Kayseri, Türkiye, 12-14 Mayıs, 2006
- [14] Sarıgöl, E. and Alemdaroğlu, N., Parametric Study on Two Dimensional Flapping Motion Proceeding of European Micro Air Vehicle Conference and Flight Competition, Braunschweig Germany, 25-26 July 2006
- [15] Jeong, J. and Hussain, F. On the Identification of a Vortex J. Fluid Mech., 285: 69-94, 1995
- [16] Chong M.S., Perry A.E. and Cantwell B.J. A General Classification of Three-Dimensional Flows *Phys. Fluids*, A2, 765, 1990.
- [17] Hunt J.C.R., Wray A.A. and Moin P., Eddies, Stream and Convergence Zones in Turbulent Flows Center for Turbulence Research Report CTR-S88, 193, 1998
- [18] Cucitore R., Quadrio M. And Baron A., On the Effectiveness and Limitations of Local Criteria for the Identification of a Vortex *Eur. J. Mech. B/Fluids*, 18 n°2, pp.261-282, 1999
- [19] Chakraborty P., Balachandar S. And Adrian R.J. On the Relationships Between Local Vortex Identification Schemes *J. Fluid Mech.*, Vol. 535, pp.189-214, 2005
- [20] Hussain A., Baig M.F. and Varshney H., Investigation of Coherent Structures in Rotating Rayleigh-Benard Convection *Phys. Fluids*, 18, 2006.
- [21] Dubief Y. And Delcayre F. On Coherent-Vortex Identification in Turbulence J. Turbulence, 1, 2000.
- [22] Kenwright D. And Haimes R. Vortex Identification Applications in Aerodynamics: a case study *Proceedings* of the 8th IEEE Visualization '97 Conference, 1997

eucass

This page has been purposedly left blank